PROCEEDINGS OF SCIENCE

Measurement of the cosmic ray iron spectrum with energy from 100 TeV to 10 PeV by LHAASO

Liqiao Yin,[a,b,*] **Suhong Chen,**[a,c] **Shoushan Zhang**[a,b] **and for LHAASO collaboration**

[a] *Institution,*
Key Laboratory of Particle Astrophysics, Institute of High Energy Physics, Chinese Academy of Science, YuQuan Road.19B, shijingshan district, Beijing, China

[b] *Institution,*
TIANFU Cosmic Ray Research Center, Chengdu, Sichuan, China

[c] *University, Department,*
University of Chinese Academy of Sciences, YuQuan Road.19A, shijingshan district, Beijing, China

E-mail: yinlq@ihep.ac.cn, chensuh@ihep.ac.cn, zhangss@ihep.ac.cn

One of the main physical goals of LHAASO is to accurately measure cosmic ray energy spectra for individual or group mass compositions. LHAASO contains four types of detectors, which can provide multiple mass sensitive observables, such as muon content, Xmax, etc. In this paper, we will focus on the steepness of the lateral distribution of the air shower. The steepness is defined as $S = D_{WCDA}/D_{KM2A}$, where D_{WCDA} is the photoelectron density of 200-220 meters from the shower axis measured by WCDA and D_{KM2A} is the particle density of 0-20 meters from the shower axis measured by KM2A. Since the lateral distribution of the iron shower is flatter than the lighter nuclei shower, the steepness is a powerful mass sensitive observable. Combined with other mass sensitive observables, LHAASO can select iron nuclei with 90% purity.

38th International Cosmic Ray Conference (ICRC2023)
26 July - 3 August, 2023
Nagoya, Japan

*Speaker

PoS(ICRC2023)419

1. Introduction

The precise measurement of fine structure on the energy spectrum of cosmic ray plays an important role in exploring the origin and acceleration of cosmic rays. Generally, there are four fine structures on the cosmic ray spectrum: "knee", "second knee", "ankle" and "GZK cutoff" [1]. They are both located above PeV and measured by ground-based detectors. The energy spectrum lower than PeV is generally recognized as a single power law with an index of -2.7. However, with the development of space exploration technology, more and more experiments, such as PAMELA, CREAM, DEMPA and so on [2], have found that there are more subtle structures in the energy spectrum. In particular, direct measurements of the proton spectrum show a hardening at $E \approx 600$ GeV and a softening at $E \approx 13$ TeV; A hardening at $E \approx 1.25$ TeV and a softening at $E \approx 34.4$ TeV on helium spectrum [3]. The current results show a highly similar structure on kinetic energy spectrum of proton and helium. The existence of these structures indicates that the same origin or acceleration of cosmic rays. Some experiments have attempted to measure that whether similar structures exist on the iron spectrum, such as VERITAS [4] [5], which is expected to find a harden at $E \approx 150$ TeV on iron spectrum but no signs up to 200 TeV. Meanwhile, it is expected that there is a softening at $E \approx 400$ TeV in iron spectrum. But there were no measurement results now.

LHAASO [6] [7] is a large composite ground-based detector array that includes four types of detectors. Vary kind of mass sensitive information in EAS can be measured, such as muon size, shower maximum, etc [8] [9]. In this study, simulation of LHAASO hybrid observation is introduced in section 2; section 3 represents the mass sensitive variables, especially *steepness*; the selection of iron and spectrum expectation is discussed in section 4; the last is the summary.

2. Simulation

2.1 Data generation

The EAS data is generated by CORSIKA 74005 version. Five components, Proton, Helium, CNO, MgAlSi and Iron are generated according to the Spectral index of -1 from 10TeV to 10PeV. The the high and low energy hadronic interaction model is QGSJET02 and FLUKA respectively. The electromagnetic interaction model is EGS4. The detector simulation of LHAASO is carried out according to reference [9], [10] and [11], which includes six telescopes, 1/2KM2A array and $1^{\#}$ pool of WCDA. For event reconstruction, the core position and arriving direction were reconstructed by KM2A and WCDA, respectively. The reconstruction method is shown in reference [12] and [13], and the reconstruction of Cherenkov images is shown in reference [14].

2.2 Hybrid event selection

For the selection of Cherenkov images, it is necessary to ensure the complete measurement of WFCTA. The single channel threshold of WFCTA camera is 50 photoelectrons. The pixels in Cherenkov image are more than 10, namely $Npix > 10$. The center of gravity of the image is within $\pm 6^{\circ}$ [9]. The distance from the shower core to the center of WFCTA array is 90-180 meters.

For selection of the shower core is shown in Fig. 1. The left figure shows core in KM2A [10] and the right figure shows core in WCDA. Two hybrid data samples are independent with each other and named S_K and S_W respectively. For S_K, the trigered EDs are more than 20 ($NTrigE > 20$).

The diffrence between the Shower-Detector-Plane (SDP) reconstruced by KM2A and WFCTA is less than 10 degree ($\delta\theta < 10°$). $\delta\theta$ can effectively eliminate the events outside the KM2A core range. This selection condition also applies to S_W samples. Moreover, the brightest cell in WCDA is greater than 300pe and the triggered cells need to be greater than 300.

After above hybrid selection, the full detection efficiency threshold of the two data samples is 150 TeV for iron spectrum analysis. The effective observation apertures are 8700 m^2Sr for S_K and 2900 m^2Sr for S_W.

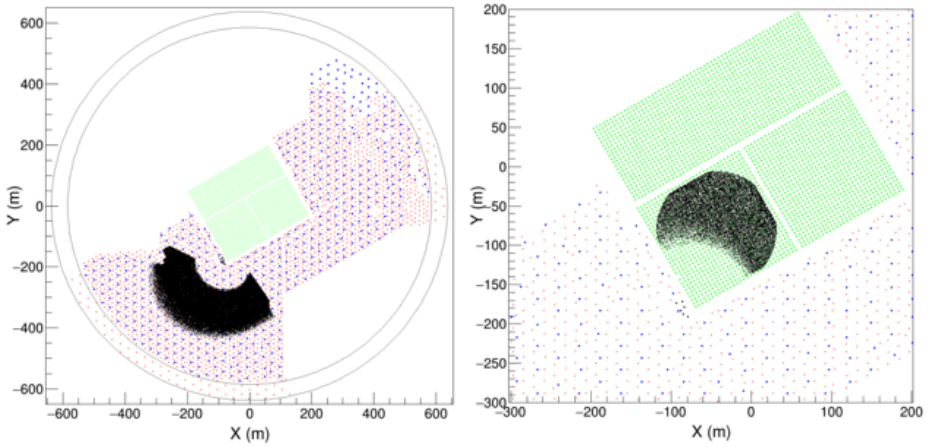

Figure 1: The shower core selection. The red and blue dots show the ED and MD in 1/2KM2A array respectively. The green dots show WCDA. The black dots show the range of shower core in KM2A (left) and WCDA (right).

2.3 Energy reconstruction

The energy reconstruction uses the size of the Cherenkov image (N_{pe}) measured by WFCTA [8]. N_{pe} gradually decreases as the distance from the shower axis (Rp) to the telescope increases. The variation slope among different primary components are inconsistent. For iron showers, the $N_{pe}-Rp$ distribution is shown in Fig. 2 (left). The normalized formula is $N^0_{pe} = log(N_{pe}) + 0.0065Rp$.

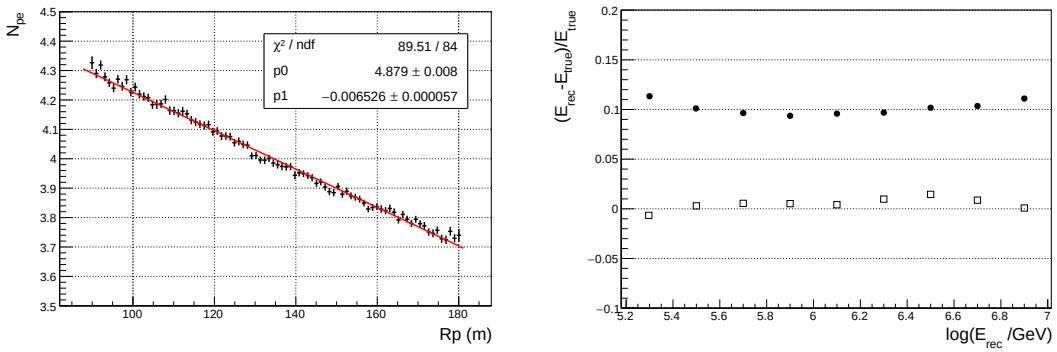

Figure 2: Left: The Cherenkov size (N_{pe}) variation with distance (Rp) for iron shower with energy above 150TeV. Right: The energy reconstruction accuracy of iron shower.

N_{pe}^0 can be used directly for energy reconstruction. The formula is $E_{rec} = 0.061(N_{pe}^0)^2 + 0.183N_{pe}^0 + 3.095$. Results are shown in Fig. 2 (right). The bias (hollow square dots) is less than ± 2% and the resolution (solid dots) is about 10%.

3. Mass Sensitive Parameters

LHAASO can provide many Mass Sensitive Parameters, such as Length/Width and Xmax in Cherenkov image, muon content, lateral distribution fluctuations in WCDA, etc. [8] [9]. Here, we have developed a new parameter related to lateral distribution.

3.1 The lateral ditribution of electromagnetic particles

As shown in Fig. 3 (left), the X-axis in the left plot is the distance to the shower axis. The distance here has been converted to the shower front. The Y-axis is the density of secondary electromagnetic particle number. It is the shower lateral distribution which can be measured by KM2A-ED. The black dots in the figure represent proton showers and the red dots represent iron showers. The difference of particle number density between proton and iron shower decreases with distance due to the coulomb scattering. Therefore, the particle number density near the shower core ($R < 20m$) can be used for particle identification.

The Fig. 3 right plot shows the lateral distribution of secondary electromagnetic particle energy, which can be measured by WCDA. The difference of particle energy density between proton and iron shower increases with distance. And the lateral distribution of proton shower is steeper than iron shower. Thus, the ratio of the particle energy density near the shower core and far from the shower core is a mass sensitive parameter.

Moreover, it is obvious that particle energy density of iron shower is larger that of proton shower, which contrary to the lateral distribution of particle number density. According to the characteristics of the two lateral distributions, the ratio of the particle number density near the shower core to the particle energy density far from the shower core can more effectively identify the primary particle species.

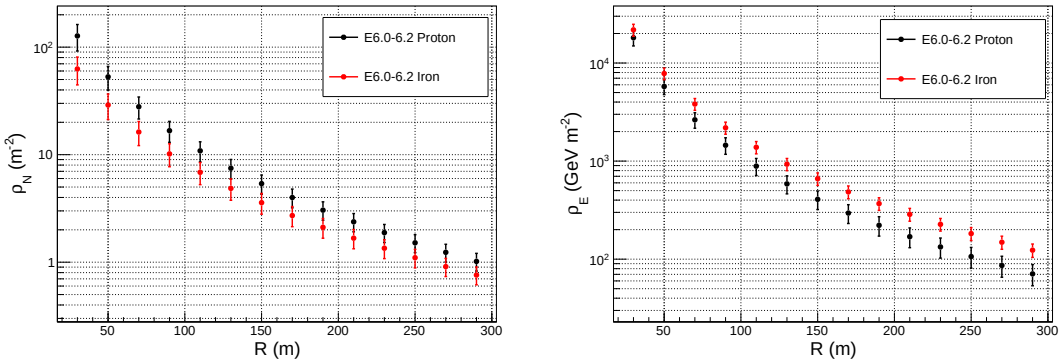

Figure 3: The lateral distribution of secondary electromagnetic particle number(left) and energy(right) form proton and iron shower.

3.2 Variable construction

This section takes S_K as a sample for discussion.

Firstly, the particle number density ρ_p within $R < 20m$ measured by KM2A-ED, should be corrected by average distance ($\bar{R}$) to shower core. ρ_p is defined as the ration of number of electromagnetic particles (N_e) and the effective detection area (A_{eff}). Since ED is a sampling array with a spacing of 15m between unit detectors, N_e will decreases with $\bar{R}$ due to the steep lateral distribution near the shower core. Here $\bar{R} = \Sigma(N_{ei} * R_i)/\Sigma(R_i)$. The correction formula is $D_{KM2A} = \rho_p + 0.08\bar{R}$, as shown in Fig. 4(left).

In addition, N_e is related to shower zenith and primary energy. After correction, an energy independent component variable ρ_{k20} is obtained. ρ_{k20}'s distribution is shown in Fig. 4 (right). Iron and other nuclei are represented by implementation and dashed lines, respectively.

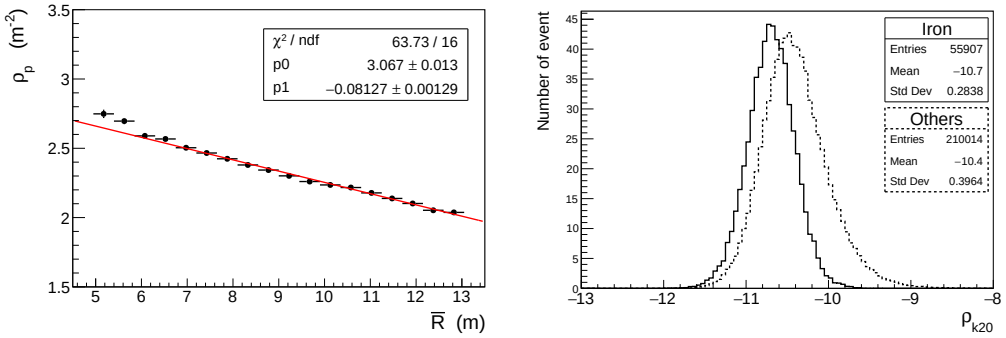

Figure 4: Left: The change of particle number density in $R < 20m$ with average distance. Right: The distribution of ρ_{k20}, with the solid line representing the iron shower and the dashed line representing other components in a ratio of 1:1.

Another mass sensitive parameter is *steepness*, which is defined as $S = D_{WCDA}/D_{KM2A}$. D_{WCDA} refers to the average photoelectron density measured by WCDA where R is in the range of 200-220m. The number of cherenkov photons in water can directly represent the energy of secondary particles. Similarly, D_{WCDA}/D_{KM2A} also varies with energy. The distribution of *steepness* after energy correction is shown in Fig. 5 (left).

When the shower core falls in the WCDA, namely the sample S_W, the ratio of the photoelectron number density with R in 20-40m and with R in 80-100m can be used to construct *steepness*, and its distribution is shown in Fig.5 (right).

4. Expection of iron sepctrum

Expectations for iron spectrum from 100TeV to 10PeV have been made through a toy simulation. Reference [2] has summarized the structure on the proton spectrum to Formula(1).

$$\Phi(E) = K\left(\frac{E}{E_0}\right)^{-\alpha_1}\left[1+\left(\frac{E}{E_b}\right)^{1/w}\right]^{-(\alpha_2-\alpha_1)w}\left[1+\left(\frac{E}{E_b'}\right)^{1/w'}\right]^{-(\alpha_3-\alpha_2)w'} \quad (1)$$

It is pushed to the iron spectrum in Z-dependent manner, and the flux is adjusted according to the Horandel model [15]. The sampling is carried out according to the red line in the Fig. 6.

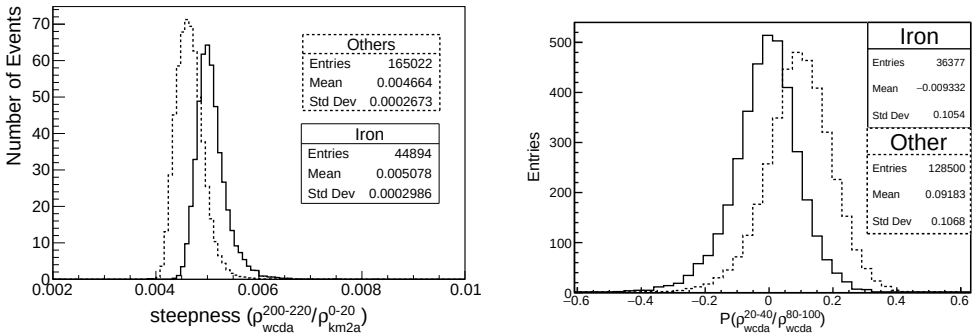

Figure 5: The distribution of *steepness* in data sample S_K (left) and S_W (right), with the solid line representing the iron shower and the dashed line representing other components in a ratio of 1:1.

The amount of data sampled is based on the current hybrid observation time (approximately 388 hours)[9]. The energy resolution is 10% and the aperture of iron is set to be $750 m_2 Sr$. If there are the fine structure in iron spectrum, LHAASO is able to complete the measurement, as shown in Fig.6(black dots). The blue line is the fit of these dot and results are shown in right frame. P3 and p6 is the position of the softening and hardening, the same with theoretical assumptions.

It should be pointed out that if the true flux of the iron is much lower than the assumption, or the fine structure is presented in the energy spectrum in an A-dependent manner, it would be necessary to use other LHAASO observation data and analysis methods to improve the statistics.

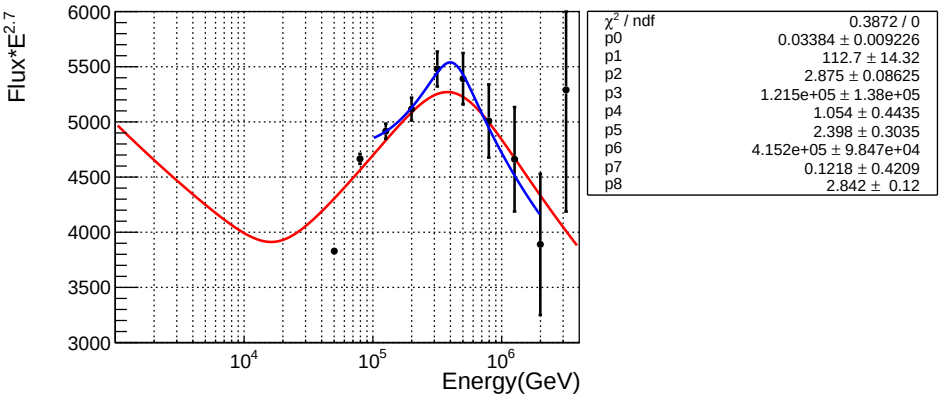

Figure 6: Expection of iron sepctrum accroding to reference [1].

5. Summary

This proceeding briefly expectation of iron spectrum from 100TeV to 10PeV according to the LhAASO hybrid observation. The lateral distribution of hybrid event are discussed in detail and three relative mass sensitive parameters are constructed. The iron identification will be executed next step research.

References

[1] NAGANO M, WATSON A A. Observations and implications of the ultrahigh-energy cosmic rays[J]. Review of Modern Physics, 2000, 72:689–732

[2] Paolo Lipari, Silvia Vernetto, The shape of the cosmic ray proton spectrum, Astroparticle Physics 120 (2020) 102441.

[3] DAMPE Collaboration, Measurement of the Cosmic Ray Helium Energy Spectrum from 70 GeV to 80 TeV with the DAMPE Space Mission,PHYSICAL REVIEW LETTERS 126, 201102 (2021).

[4] Henrike Fleischhack for the VERITAS collaboration, A template method for measuring the iron spectrum in cosmic rays with Cherenkov telescopes, arXiv:1508.05823v1 [astro-ph.IM] 24 Aug 2015, ICRC2015.

[5] Henrike Fleischhack for the VERITAS collaboration, Measurement of the Iron Spectrum in Cosmic Rays with VERITAS, ICRC2017, arXiv:1708.02960v2 [astro-ph.HE] 25 Sep 2017.

[6] Z. Cao (for LHAASO Coll.), Chin.Phys. C, 2010, (34)249-252.

[7] Z. Cao et al., Introduction to Large High Altitude Air Shower Observatory (LHAASO), Chinese Astronomy and Astrophysics, 2019, 43: 457-478.

[8] L. Q. Yin et. al for for the LHAASO Collaboration, Expected energy spectrum of cosmic ray protons and helium below 4 PeV measured by LHAASO, Chinese Physics C Vol. 43, No. 7 (2019) 075001.

[9] Ma Lingling, Wang Yudong, Wang Liping, Yin Liqiao, You Zhiyong, and Zhang Shoushan on behalf of the LHAASO Collaboration, Measurement of the cosmic ray proton and helium spectrum with energy above 100TeV by the LHAASO experiment, PoS(ICRC2021)377.

[10] Liping Wang et. al for for the LHAASO Collaboration, Cosmic ray mass independent energy reconstruction method using Cherenkov light and muon content in LHAASO, PHYSICAL REVIEW D 107, 043036 (2023).

[11] Aharonian, F. et al. for the LHAASO Collaboration, Calibration of the air shower energy scale of the water and air Cherenkov techniques in the LHAASO experiment, PHYSICAL REVIEW D, 2021, 104(6): 0-062007.

[12] Aharonian, F. et al. for the LHAASO Collaboration, Observation of the Crab Nebula with LHAASO-KM2A for the performance study, Chinese Physics C 45.2(2021):025002.

[13] Aharonian, F. et al. for the LHAASO Collaboration, Performance of LHAASO-WCDA and observation of the Crab Nebula as a standard candle, Chinese Physics C, Vol. 45, No. 8 (2021) 085002.

[14] F. Aharonian et al. for the LHAASO Collaboration, Reconstruction of Cherenkov image by multiple telescopes of LHAASO-WFCTA, Radiation Detection Technology and Methods (2022) 6:544–557.

[15] Johannes Blümer, Ralph Engel, Jörg R.Hörandel, Progress in Particle and Nuclear Physics 63(2009) 293-338.